

# Probing anisotropic mechanical behaviour in Carbamazepine Form III

Benjamin P. A. Gabriele<sup>a</sup>, Craig J. Williams<sup>b</sup>, Matthias E. Lauer<sup>c</sup>, Brian Derby<sup>b</sup>, Aurora J. Cruz-Cabeza<sup>a\*</sup>

<sup>a</sup> School of Chemical Engineering and Analytical Science, University of Manchester, UK.

<sup>b</sup> School of Materials, University of Manchester, UK.

<sup>c</sup> Roche Innovation Center Basel, Basel, Switzerland

\*Email: [aurora.cruzcabeza@manchester.ac.uk](mailto:aurora.cruzcabeza@manchester.ac.uk)

**Abstract:** This Electronic Supplementary Information (ESI) includes precisions and additional results from powder x-ray diffraction measurements, nanoindentation experiments, computations and molecular dynamic simulations.

## S1. Experimental Methods

**Powder X-Ray Diffraction.** Face indexing presented in the main manuscript was further confirmed using *preferential orientation* Powder X-Ray Diffraction (PXRD, D2-Phaser, Bruker). Four to six single crystals of carbamazepine form III, grown from methanol, were placed at room temperature on the PXRD stage, with their largest face pointing up. The diffractometer was equipped with a Cu x-ray source ( $\lambda = 1.54184 \text{ \AA}$ ), emitting at 10mA and 30kV. Measurements were carried with over a range 2 $\theta$  of 5 – 40° with a step increment of 0.02°.

**Nanoindentation.** Experiments were carried out using a Hysitron Ti950 Triboindenter (Hysitron/Bruker) equipped with a diamond Berkovich probe, in load-control mode using a unique trapezoid load function: 5 second load, 2 second hold and 5 seconds unload segments. The maximum load  $P_{MAX}$  used was fixed to 3mN. Results from indenting CBZ-III single crystals led to load-depth traces containing sudden bursts, commonly called pop-ins. Their intensities were manually measured and compared as histograms to assess possible trends.

**Mechanical properties.** The Young's modulus of CBZ-III, using the CSD refcode CBMZPN02, was computed as described in the experimental section in the associated main manuscript. The matrices of elastic stiffness and compliance are here presented. The Young's modulus was computed for all 3D directions of space using the EIAM computer program,<sup>1</sup> and the value corresponding to each indentation direction was hence assessed.

### Computations.

*Calculation of Lattice energy.* Using the software Material Studio 2019 (Dassault Systèmes, BIOVIA),<sup>2</sup> the energy associated with the unit cell of carbamazepine form III (CSD refcode: CBMZPN02) was first calculated by relaxing the atoms positions using the forcefield COMPASSII (with its own forcefield charges) while keeping the unit cell parameters constants. The crystal energy was then normalised by the number of molecules in the unit-cell ( $U_{CRYSTAL}$ ). A separate simulation was carried out in which a single molecule of carbamazepine was fully optimised in the gas phase ( $U_{GAS}$ ). The lattice energy  $U_{LATT}$  was then calculated as  $U_{LATT} = U_{CRYSTAL} - U_{GAS}$ . The electrostatic and the Van der Waals contributions towards  $U_{LATT}$  were then calculated as  $U_{LATT-ELEC} = U_{CRYSTAL-ELEC} - U_{GAS-ELEC}$  and  $U_{LATT-VdW} = U_{CRYSTAL-VdW} - U_{GAS-VdW}$ .

*Simulation of compressions.* Using the same software and with the same level of theory, the compression normal to the (020) plane was simulated as follows: the length of the unit cell parameter  $b$  was stepwise reduced by 0.1 Å, whilst the  $a$  and  $c$ -axes were kept constant (Figure S1.1). For each

step,  $U_{CRYSTAL-B}$  was computed by relaxing the atoms positions (as mentioned above) and the lattice energy for the compressed system was calculated as  $U_{LATT-B} = U_{CRYSTAL-B} - U_{GAS}$ . Additionally, for each step the angle  $\theta$  between the two external rings was measured (Figure S1.1b). The same procedure was repeated while keeping rigid all the flexible bonds of all the molecules in the unit cell (Figure S1.1c), hence in this final step, the angle is kept constant  $\theta = \theta_0$ .

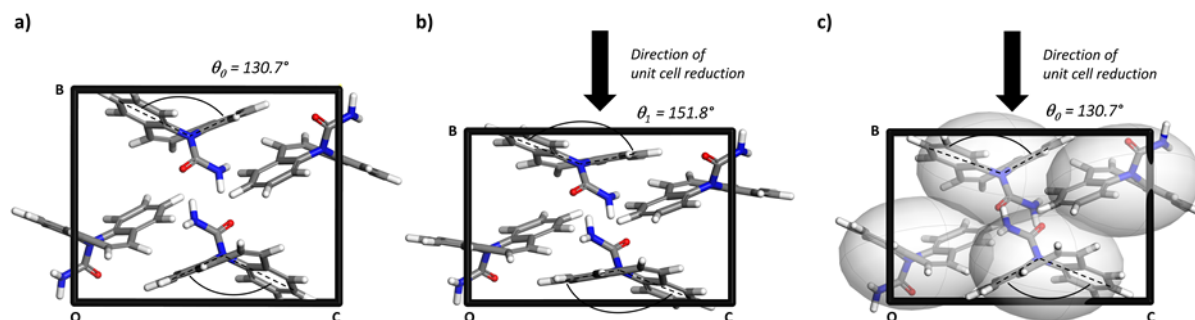


**Figure S1.1:** (a) Unit cell of carbamazepine form III from CSD refcode CBMZPN02, after geometry optimisation without unit cell optimisation.  $\theta_0$  is the angle between the two external rings of a molecule of carbamazepine. This angle was measured between the normal of each ring as shown in the main manuscript, Figure 0. Here, such angle is shown between the dashed lines. (b) Unit cell after manual reduction of the b-axis to  $b = 9 \text{ \AA}$ . Atoms positions were relaxed and the structure optimised, hence the angle between the two external rings increased. (c) Unit cell after manual reduction of the b-axis to  $b = 9 \text{ \AA}$  while keeping rigid the flexible bonds, hence the angle remained to its initial value.

These steps were first repeated while simulating a compression normal to the (002) plane, i.e. where the c-axis was stepwise reduced by  $0.1 \text{ \AA}$  per reduction step whilst the a and b-axes were kept constant. The lattice energy  $U_{LATT-C}$ , the *CED* and the angle  $\theta$  were monitored.

A final set of calculation was carried out while simulating a compression normal the (101) plane, however to determine the axes reduction was not straightforward. Figure S1.2 shows a simple sketch to explain how this was achieved. While indenting the (101) plane, the angle  $\beta$  was assumed to remain constant and the plane (101) assumed to remain orthogonal to the indentation direction. Using Thales theorem:

$$\frac{OA}{OA_1} = \frac{OC}{OC_1} = \frac{AC}{A_1C_1} \quad (\text{S1})$$

$OA_1$  and  $OC_1$  are the values to define the new unit cell upon compression. Hence, simulation of a compression normal to (101) can be achieved by reducing stepwise the a and c-axes of the same percentage. For each reduction step,  $U_{LATT-101}$ , the *CED* and the angle  $\theta$  were monitored.

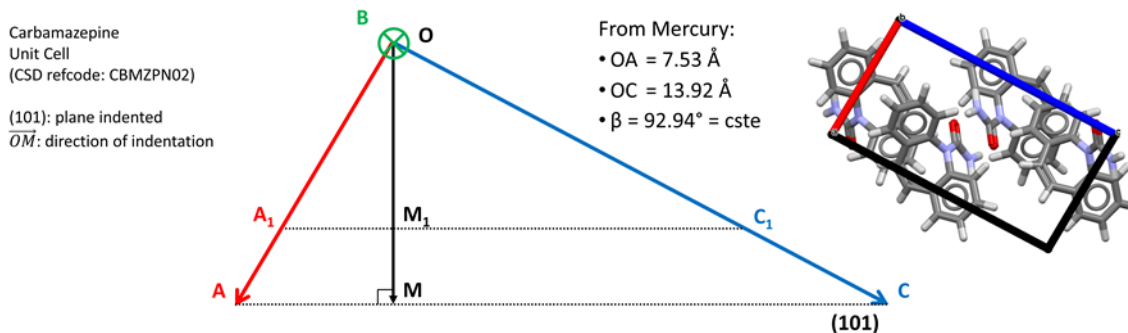


**Figure S1.2:** Unit cell of carbamazepine form III from CSD refcode CBMZPN02, with the (101) plane. Compression was simulated by the reduction of the a and c-axes. The angle  $\beta$  was kept constant, and  $[A_1C_1]$  remains orthogonal to the indentation direction  $[OM]$ , hence  $A_1$  and  $C_1$  values can be determined using Thales' theorem (Intercept theorem).

**Molecular Dynamics – Shearing simulations.** Supercells of 96 molecules of carbamazepine form III were generated from the unit cell that had undergone atoms relaxation as explained above (see Computation). The supercells were first let to equilibrate for 50 picoseconds at 298 kelvins while keeping temperature and volume constant (*NVT*) before equilibrating the supercells further for 50 picoseconds while keeping pressure and temperature constant instead (*NPT*). Hence, parallel shearing simulations were carried out at  $T = 298\text{K}$  at constant shear rate =  $5 \cdot 10^{-4} \text{ ps}^{-1}$  for 1500ps (*NVT*). In each simulation, a pure shear force was applied along one of the supercell axes which corresponds to the direction of indentation. Shearing simulations are made such that one plane must be kept constant. We limited this study to two simulations per indentation direction, hence two fixed planes, chosen orthogonal to each other. Note the special configurations imposed by the indentation of the (101) plane, which corresponds to a direction of indentation parallel to  $[301]$ . This is first explained in Figure S1.2 and further detailed in this ESI (see Figures S4.1 and S4.2). For each simulation, the activated slip system (i.e slip plane + slip direction) in the supercell was observed and is reported in the main manuscript. Additional images of the shearing for each simulation are presented in this ESI.

## S2. Powder X-ray diffraction patterns

To confirm the face indexing carried out via Single Crystal X-Ray Diffraction (SCXRD), 4 to 6 single crystals were used in Powder X-Ray Diffraction experiments. Crystals were placed flat on the stage, their largest face pointing up. This experiment, sometimes referred to as *Preferential Orientation PXRD*, enabled to see the diffraction peaks associated with the largest faces only, hence to identify those by comparing their diffraction angle with the corresponding reference (CSD refcode, here CBMZPN02).<sup>3</sup> Results are shown in Figure S2 and Table S2. The peaks obtained match very well those identified with SCXRD.

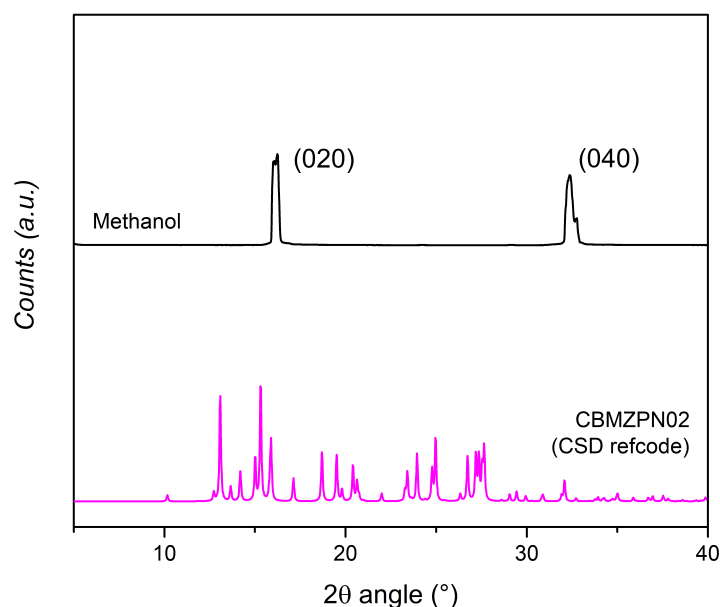


**Figure S2:** Powder X-Ray Diffraction (PXRD) patterns obtained on single crystals of CBZ-III crystallised from methanol (black line). The crystals were placed on the stage with their dominant face facing up. The reference pxrd pattern from the CSD refcode (CBMZPN02) is shown as well (pink line). Preferential orientation is revealed as (020). The positions of the peaks were matched with the corresponding peak on the reference to carry out the indexing.

**Table S2:** Angle and (*hkl*) face associated with the peaks obtained from preferential orientation PXRD on single crystals grown from methanol, isopropanol or ethyl acetate. Good match was obtained for all peaks with those from the CSD refcode CBMZPN02, used as a reference.

Solvent / Reference	Peak 1, Angle° (Crystal face, <i>hkl</i> )	Peak 2, Angle° (Crystal face, <i>hkl</i> )
Methanol	16.24 (020)	32.38 (040)
Reference	16.12 (020)	32.08 (040)

### S3. Nanoindentation

The trapezoid load-function used for the indentation of carbamazepine single crystals is presented hereafter in Figure S3.1.

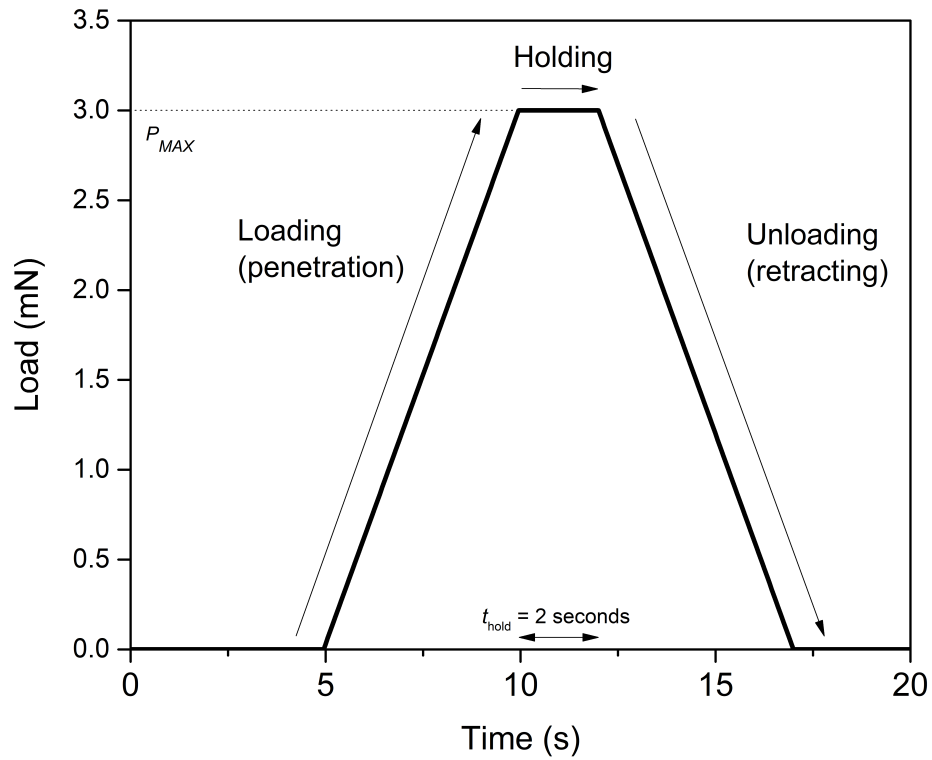


**Figure S3.1:** The trapezoid load function used on indenting CBZ-III single crystals (load-controlled mode).

Upon indenting CBZ-III single crystals, several pop-ins were observed on the load-depth traces, with between 5 to 10 events per curve. Their intensities – measured as the absolute difference in depth before and after the burst, is shown in Figure S3.2. Several studies of nanoindentation on molecular single crystals reported that the intensity of pop-ins matched crystallographic dimensions such as one particular unit cell length or interplanar spacing, due to the slip of crystal planes along this orientation.<sup>4-6</sup> However, we could not establish here such conclusion. In Figure S3.2, no bar is significantly higher to establish this conclusion with certainty.

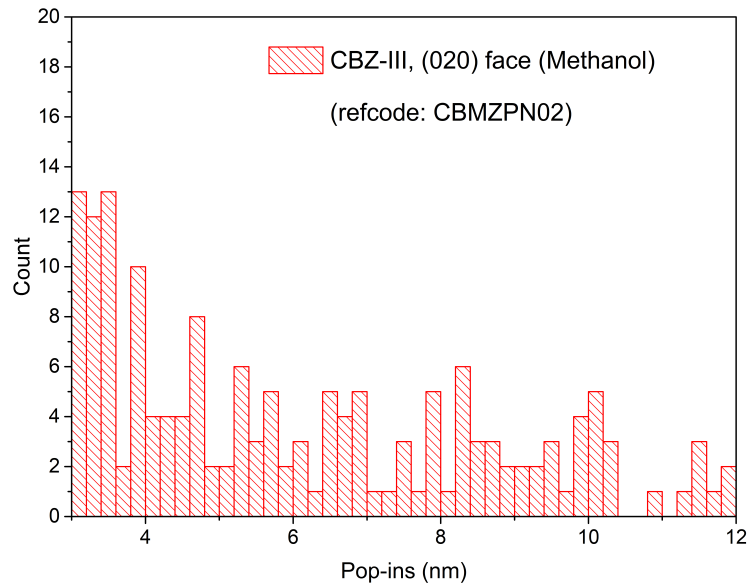


**Figure S3.2:** Histograms of the count of the pop-ins intensities across the 90 indentation measurements carried out on 10 single crystals of CBZ form III grown from methanol. No correlation was found between these data and any interplanar spacing using CSD refcode CBMZPN02.

Figures S3.3 shows a histogram representation of the  $E_R$  and  $H$  values obtained from the nanoindentation experiments on CBZ-III single crystals.

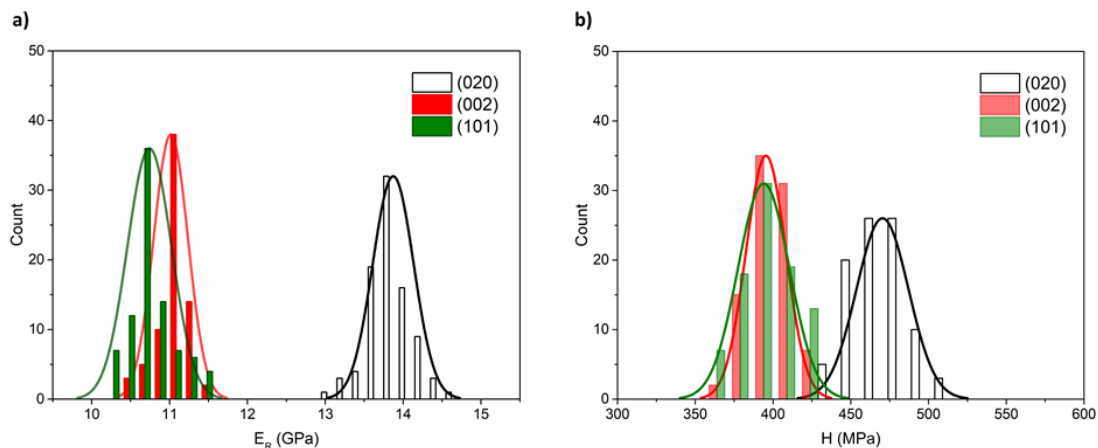


**Figure S3.3:** Histograms of reduced modulus  $E_R$  (a) and hardness  $H$  (b) comparing measurements obtained on single crystals of carbamazepine form III grown from methanol, carried out separately on (020), (101) and (002) faces. A normal distribution curve has been added on top of each dataset for visualisation purposes only.

#### S4. Mechanical properties results

The stiffness and compliance matrices of CBZ-III calculated from *MD*-simulations results, without structure optimisation, are (expressed respectively in GPa and GPa<sup>-1</sup>):

$$C_{COMP-RT} = \begin{pmatrix} 14.69 & 4.94 & 5.47 & 0 & -2.96 & 0 \\ 4.94 & 12.20 & 1.88 & 0 & 0.28 & 0 \\ 5.47 & 1.88 & 9.46 & 0 & -1.08 & 0 \\ 0 & 0 & 0 & 3.34 & 0 & -0.85 \\ -2.96 & 0.28 & -1.08 & 0 & 5.61 & 0 \\ 0 & 0 & 0 & -0.85 & 0 & 4.55 \end{pmatrix}$$

$$S_{COMP-RT} = \begin{pmatrix} 0.110 & -0.038 & -0.050 & 0 & 0.050 & 0 \\ -0.038 & 0.098 & 0 & 0 & -0.025 & 0 \\ -0.050 & 0 & 0.135 & 0 & 0 & 0 \\ 0 & 0 & 0 & 0.314 & 0 & 0.059 \\ 0.050 & -0.025 & 0 & 0 & 0.206 & 0 \\ 0 & 0 & 0 & 0.059 & 0 & 0.231 \end{pmatrix}$$

The stiffness and compliance matrices of CBZ-III calculated from *MD*-simulations results, with structure optimisation, are (expressed respectively in GPa and GPa<sup>-1</sup>):

$$C_{COMPT-0K} = \begin{pmatrix} 18.99 & 8.84 & 10.14 & 0 & -1.81 & 0 \\ 8.84 & 20.84 & 8.01 & 0 & 1.73 & 0 \\ 10.14 & 8.01 & 18.94 & 0 & 1.39 & 0 \\ 0 & 0 & 0 & 5.62 & 0 & -1.46 \\ -1.81 & 1.73 & 1.39 & 0 & 7.14 & 0 \\ 0 & 0 & 0 & -1.46 & 0 & 5.41 \end{pmatrix}$$

$$S_{COMPT-0K} = \begin{pmatrix} 0.089 & -0.026 & -0.040 & 0 & 0.036 & 0 \\ -0.026 & 0.065 & -0.012 & 0 & -0.020 & 0 \\ -0.040 & -0.012 & 0.081 & 0 & -0.023 & 0 \\ 0 & 0 & 0 & 0.191 & 0 & 0.052 \\ 0.036 & -0.020 & -0.023 & 0 & 0.159 & 0 \\ 0 & 0 & 0 & 0.052 & 0 & 0.199 \end{pmatrix}$$

Using the matrix  $S$ , the Young's modulus along the three main axes can be defined as:

$$E_X = \frac{1}{S_{11}} \quad (\text{S4.1})$$

$$E_Y = \frac{1}{S_{22}} \quad (\text{S4.2})$$

$$E_Z = \frac{1}{S_{33}} \quad (\text{S4.3})$$

The EIAM software converts the matrix  $S$  (assumed to be defined in the base  $X, Y, Z$ ) into  $S'$  defined for different sets of base vectors  $X', Y', Z'$ , such that the Young's modulus along the new  $x'$  vector

$$E_{X'} = \frac{1}{S_{1'1'}} \quad (\text{S4.4})$$

There is no need to compute  $E_{Y'}$  or  $E_{Z'}$  because the matrix  $S$  is successively defined such that the new  $X'$  vectors will span the entire 3-dimensional space. From this, the Young's modulus of CBZ-III is calculated for each dimension in 3D (see the graphs in Figure 7 in the main manuscript). We reasonably assumed that experimental values  $E$  obtained on (020) and (002) faces can be compared with  $E_Y = E_{010}$  and  $E_Z = E_{001}$ . However, the [101] direction is not orthogonal to the (101) plane because for CBZ-III, i) the corresponding crystal system is monoclinic and ii) the  $a$  and  $c$ -axes have different lengths. This is further explained in Figures S4.1 and S4.2. In these figures, the direction normal to the (101) plane is parallel [OX], from which the closest direction is [301] as seen in Figure S4.2.

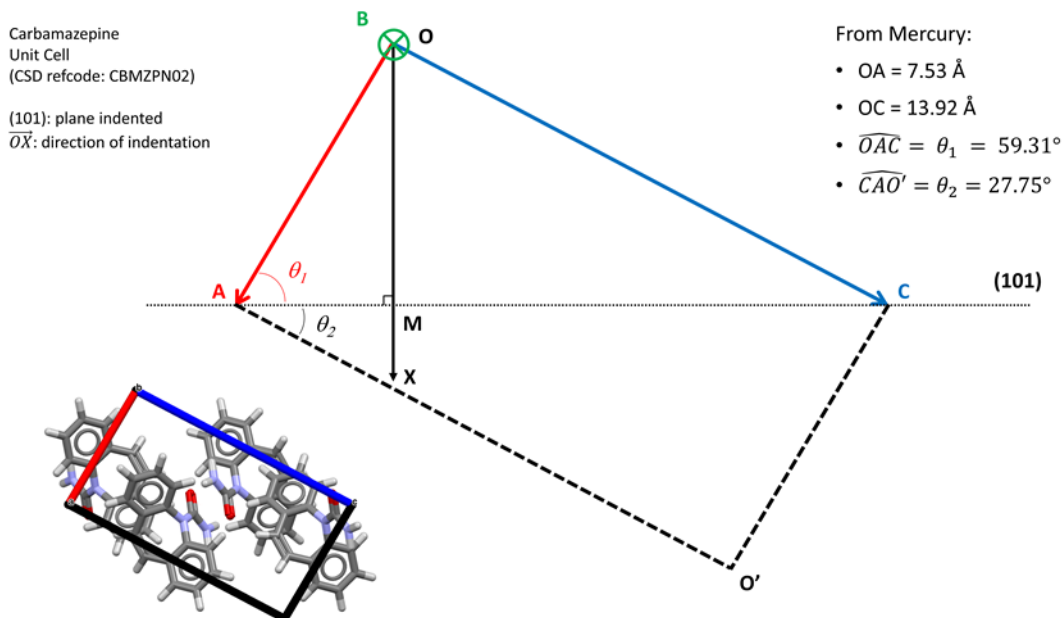


**Figure S4.1:** Carbamazepine Form III (from CSD refcode CBMZPN02) unit cell. The (101) plane, largest face for crystals grown from ethyl acetate, is represented by the horizontal dashed line, hence the indentation direction is its normal (parallel to  $\vec{OX}$ ).

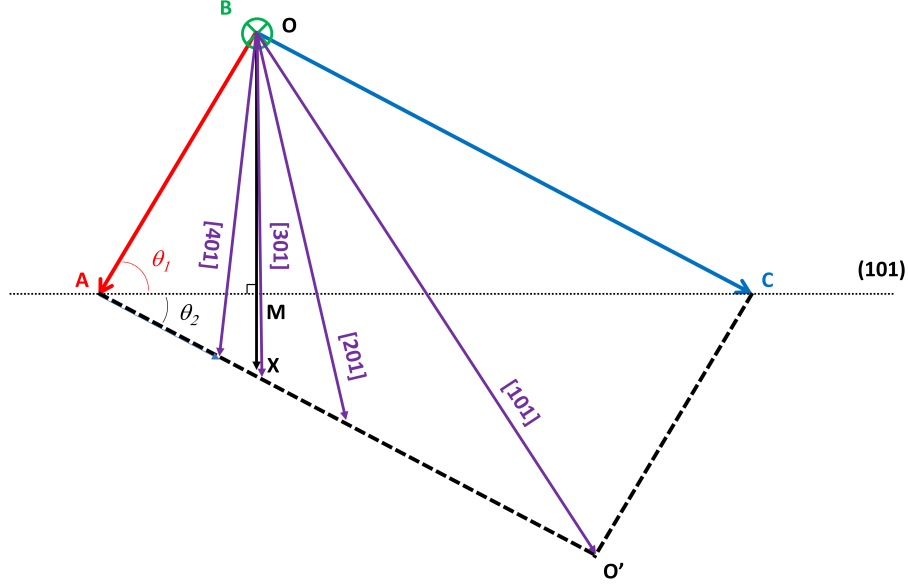


**Figure S4.2:** Carbamazepine Form III unit cell showing the [101], [201], [301] and [401] directions. The direction indented is parallel to  $\overline{OX}$ , hence [301] is the closest direction parallel to the indentation direction.

## S5. Elastic modulus from energy potential well

We assume a potential well of the following form:

$$U_{LATT} \cong k_0 + k_1x + k_2x^2 \quad (\text{S5.1})$$

This assumption can be considered true only i) close to  $U_{LATT-MIN}$  and ii) for small variations of strain values, so for small variations of  $x$  in Equation S6 around  $x_{MIN} = x_0$ . Using Equation S6, The Young's modulus  $E$  can be theoretically deduced from the potential energy between molecules using Hooke's law:

$$\sigma = E \cdot \varepsilon \rightarrow E = \frac{\sigma}{\varepsilon} \approx \frac{d\sigma}{d\varepsilon} = \frac{d\left(\frac{F}{A}\right)}{d\left(\frac{dx}{x_0}\right)} = \frac{x_0}{A} \frac{dF}{dx} = \frac{x_0}{A} \frac{d^2U_{LATT}}{dx^2} = \frac{x_0}{A} \times 2k_2 \quad (\text{S5.2})$$

With  $x_0$  the distance between molecules at  $U_{LATT} = U_{LATT-MIN}$ ,  $A$  the surface area compressed and  $k_2$  the coefficient as defined in Equation S6. We see that  $E$  is proportional to  $k_2$ , however,  $x_0$  and  $A$  vary with the direction of compression. Given that  $U_{LATT}$  was computed twice for each direction of compression – whilst keeping the molecules flexible and rigid – we first fitted the computed lattice energy functions around  $U_{LATT-MIN}$  (Figure S5) and compare  $k_{2-RIGID}$  and  $k_{2-FLEXIBLE}$  values, for equivalent direction of compression only: by doing so,  $x_0$  and  $A$  can be considered as constant.

In Table S5, for each line, the value of  $k_2$  is always lower when considering flexible molecules. Considering  $E$  proportional to  $k_2$ , it indicates that in CBZ-III, flexibility makes the crystal less stiff (lower values of  $E$  than for a theoretical crystal made of rigid CBZ molecules).

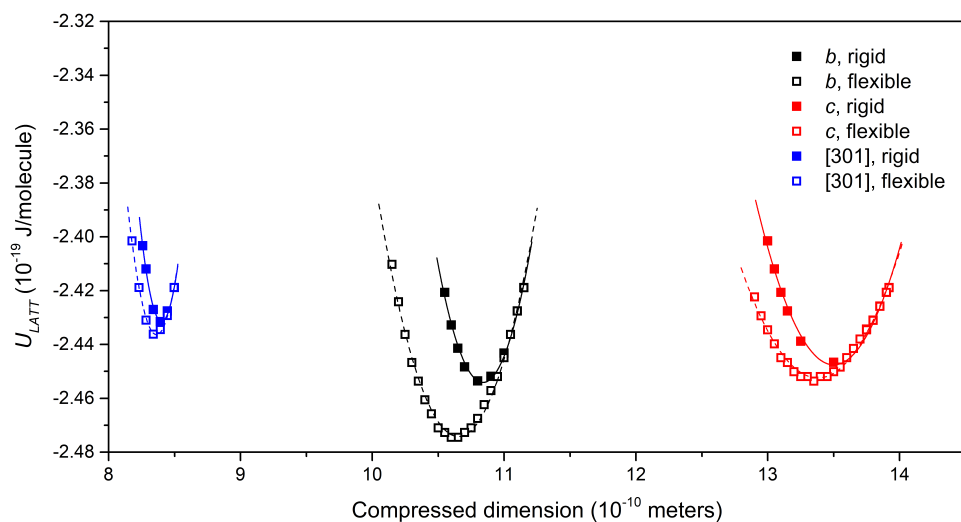


**Figure S5:** Lattice energy functions as a function of the compressed dimension, for compressions along [010], [001] and [301].  $U_{LATT}$  values were calculated for each direction with molecules maintained either rigid or flexible. Only data around  $U_{LATT-MIN}$  are shown, and were fitted with a second order polynomial function, for which the coefficient  $k_2$  are shown in Table S5.

**Table S5:**  $k_2$  coefficients extracted from the lattice energy functions for three directions of compressions considered in the associated simulations.

<b><i>X</i> – direction of compression</b>	<b><math>k_2</math> (rigid, J/m<sup>2</sup>)</b>	<b><math>k_2</math> (flexible, J/m<sup>2</sup>)</b>
[010]	3.8	2.4
[001]	1.74	1.21
[301]	13.9	10

## S6. Lattice energy calculation

The lattice energy  $U_{LATT}$  along with the non-bonded electrostatic and Van der Waals energy contributions are presented in the following Table:

	<b>Total (kJ/mol)</b>	<b>Electrostatic contribution (kJ/mol)</b>	<b>Van der Waals contribution (kJ/mol)</b>
$U_{CRYSTAL}$	-289.3	-308.7	-67.9
$U_{GAS}$	-143.6	-278.9	46.3
$U_{LATT}$	-145.7	-29.8	-115.8

### S7. MD-shearing simulation results.

Images of the supercells of each simulation, before and right after the slip event occurred, are presented in Figure S7.1-3. Some molecules were highlighted to emphasize the slip event. The shear direction is orthogonal to the faces indented as presented in the main manuscript, i.e. orthogonal to (020), (002) and (101). Note that for each shearing condition, supercells of different volumes were created and simulations were carried out on each supercell. Different supercell volumes led to the observation of the same slip system. For a good visualisation, the images in Figure S7.1-3 show the results of simulations where slip occurred through the middle of the supercell.

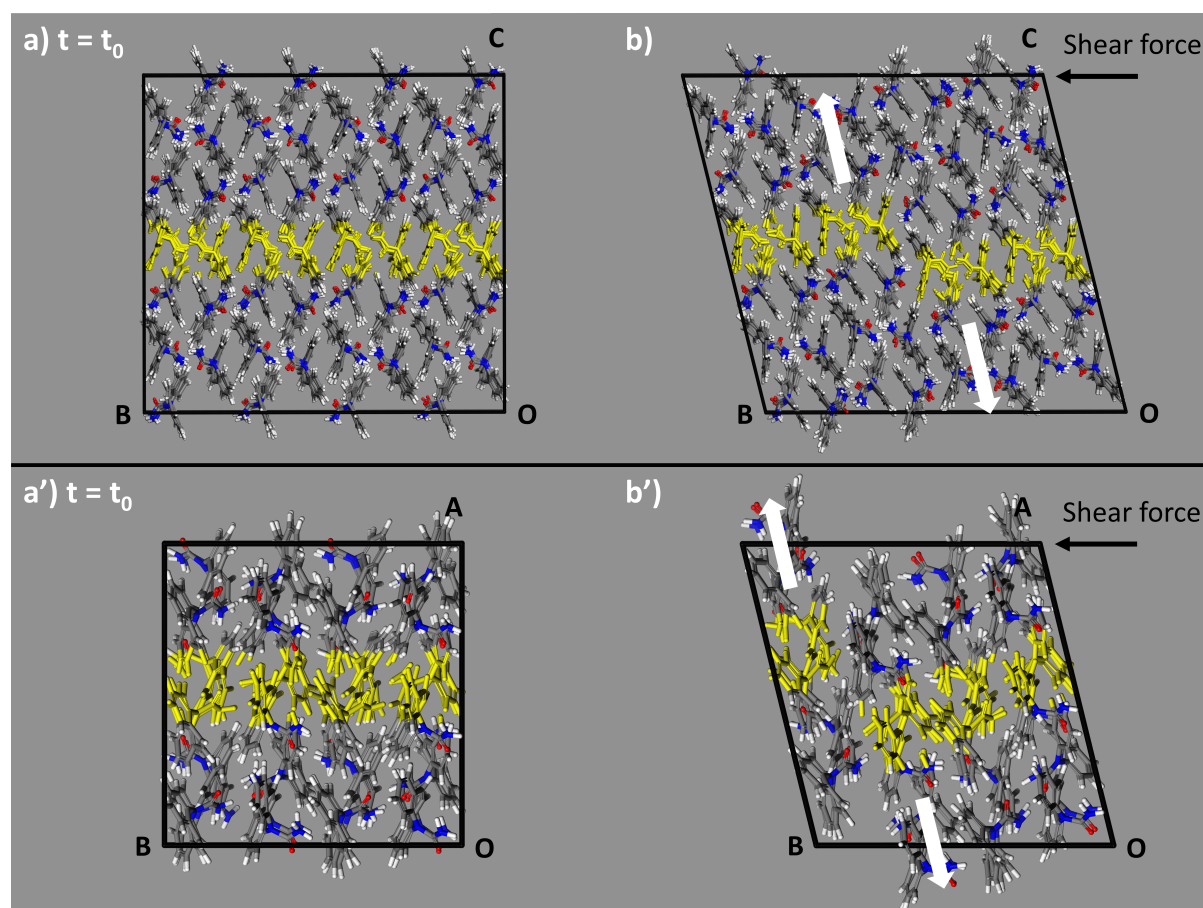


**Figure S7.1:** Annotated supercells during *MD*-shearing simulations, shear direction parallel to [010]. (a and a') Supercell at the initial state (prior to the application of the shear force) (b) Keeping the bottom (BOA) plane constant, sheared supercell right after the first slip event occurred along the slip system (020)[001]. Some molecules were highlighted in yellow to improve visualisation. (b') Keeping the bottom (BOC) plane constant, sheared supercell right after the first slip event occurred along the slip system (020)[100]. Some molecules were highlighted in yellow to improve visualisation.

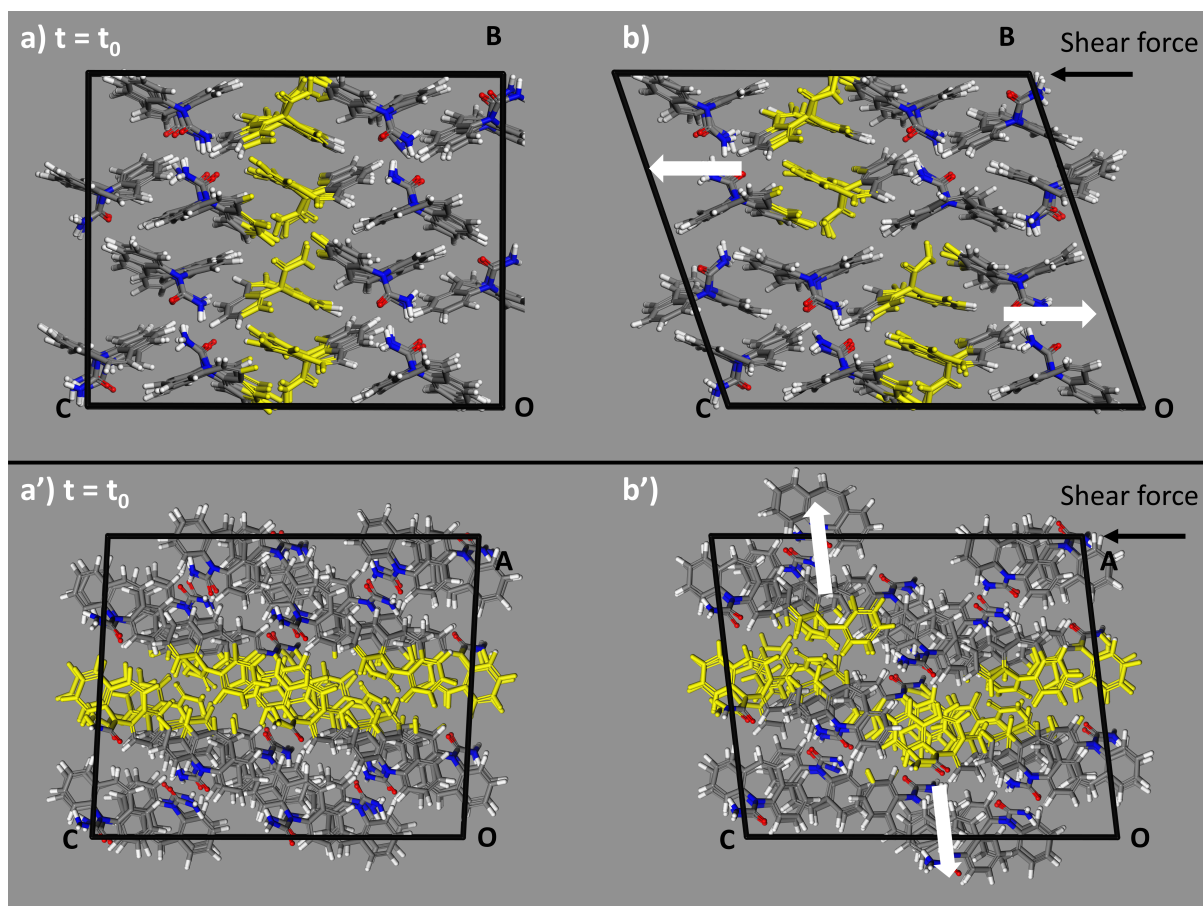


**Figure S7.2:** Annotated supercells during *MD*-shearing simulations, shear direction parallel to  $[001]$ . (a and a') Supercell at the initial state (prior to the application of the shear force) (b) Keeping the bottom (COA) plane constant, sheared supercell right after the first slip event occurred along the slip system  $(020)[001]$ . Some molecules were highlighted in yellow to improve visualisation. (b') Keeping the bottom (COB) plane constant, sheared supercell right after the first slip event occurred along the slip system  $(002)[100]$ . Some molecules were highlighted in yellow to improve visualisation.

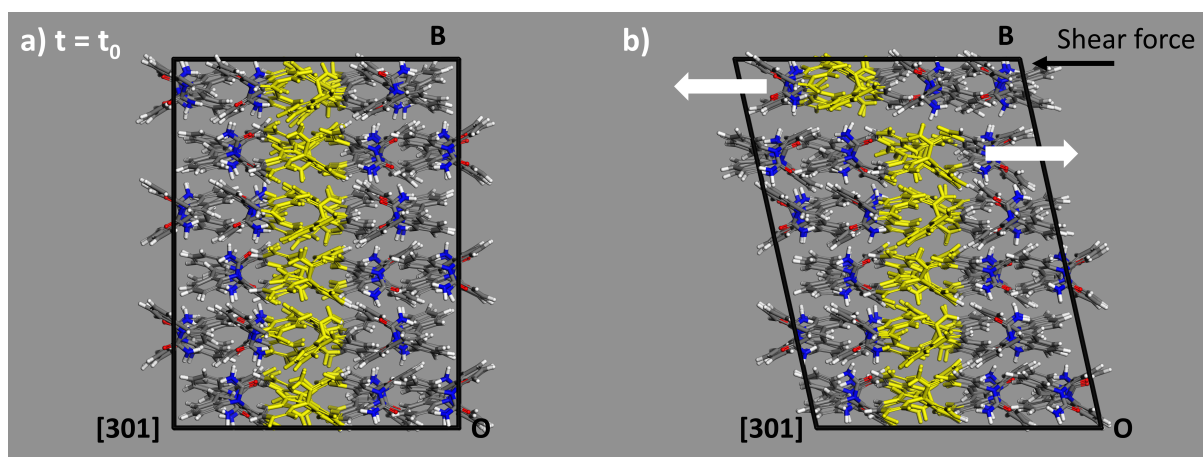


**Figure S7.3:** Annotated supercells during *MD*-shearing simulations, shear direction parallel to  $[301]$ , direction orthogonal to  $(101)$  plane. (a) Supercell at the initial state (prior to the application of the shear force) (b) Keeping the bottom  $(020)$  plane constant (here defined by  $[301]$ , the origin  $O$  and the normal direction  $[-101]$ ), sheared supercell right after the first slip event occurred along the slip system  $(020)[301]$ . Some molecules were highlighted in yellow to improve visualisation.

## References

- (1) Marmier, A.; Lethbridge, Z. A. D.; Walton, R. I.; Smith, C. W.; Parker, S. C.; Evans, K. E. ELAM: A Computer Program for the Analysis and Representation of Anisotropic Elastic Properties. *Comput. Phys. Commun.* **2010**, *181*, 2102–2115.
- (2) Dassault Systèmes BIOVIA, Materials Studio, Release 2019, San Diego: Dassault Systèmes. **2019**.
- (3) Lisgarten, J. N.; Palmer, R. A.; Saldanha, J. W. Crystal and Molecular Structure of 5-Carbamyl-5H-Dibenzo[b,f] Azepine. *J. Crystallogr. Spectrosc. Res.* **1989**, *19*, 641–649.
- (4) Kiran, M. S. R. N.; Varughese, S.; Reddy, C. M.; Ramamurty, U.; Desiraju, G. R. Mechanical Anisotropy in Crystalline Saccharin: Nanoindentation Studies. *Cryst. Growth Des.* **2010**, *10*, 4650–4655.
- (5) Varughese, S.; Kiran, M. S. R. N.; Solanko, K. A.; Bond, A. D.; Ramamurty, U.; Desiraju, G. R. Interaction Anisotropy and Shear Instability of Aspirin Polymorphs Established by Nanoindentation. *Chem. Sci.* **2011**, *2*, 2236–2242.
- (6) Mishra, M. K.; Ramamurty, U.; Desiraju, G. R. Solid Solution Hardening of Molecular Crystals: Tautomeric Polymorphs of Omeprazole. *J. Am. Chem. Soc.* **2015**, *137*, 1794–1797.